Osteoporos Int (1998) 8:317–325

Osteoporosis International

Original Article

Image-Based Assessment of Spinal Trabecular Bone Structure from High-Resolution CT Images

C. L. Gordon, T. F. Lang, P. Augat and H. K. Genant

Osteoporosis and Arthritis Research Group, Department of Radiology, University of California, San Francisco, USA

Abstract. The goal of this study was to assess whether a high-resolution CT measure of trabecular bone structure can enhance the discrimination between subjects with or without a vertebral fracture and having overall low hip or spine bone mineral density (BMD) by dual-energy X-ray absorptiometry (DXA). Sixty-one women with low BMD by DXA (*T*-score <–2.5 at hip or spine) were examined. Twenty women had sustained a vertebral fracture. Quantitative CT (QCT) BMD and high-resolution CT spinal scans were performed on a whole-body CT scanner. For the high-resolution images (0.31 mm pixel, 1.5 mm thick slice), trabecular bone was segmented from marrow using an adaptive threshold, region growth and skeletonization step. From the processed image we measured the apparent trabecular bone fraction (BV/TV), apparent trabecular thickness (I.Th) and apparent trabecular spacing (I.Sp). We also assessed the connectivity of the marrow space using region growing to derive a mean (H_A) and maximum (H_M) hole size. Despite the fact that the study population was preselected to have a low BMD by DXA, QCT BMD was highly associated with (p <0.005) with fracture status. All structural parameters were correlated (r ~ 0.64 to 0.79) with BMD with p <0.003 and showed significant differences between the fracture and non-fracture group. However, except for H_A, this difference did not remain significant after adjustment for BMD. When BMD and then H_A was entered into a paired linear regression model to predict fracture outcome, H_A contributed with p = 0.03 and BMD with p = 0.86. ROC analysis was applied and showed that H_A, BMD, I.Th and I.Sp discriminated the two groups with areas of 0.76, 0.75, 0.71 and 0.68, respectively. These findings suggest that an assessment of vertebral trabecular structure from high-resolution CT images is useful in discriminating subjects with vertebral fractures and potentially useful for predicting future fractures.

Keywords: Connectivity; High-resolution CT; Trabecular structure; Vertebral fracture

Correspondence and offprint request to: Christopher Gordon, PhD, Osteoporosis and Arthritis Research Group, University of California, San Francisco, Department of Radiology, Box 1250, San Francisco, CA 94143, USA. Tel: +1(415) 476-5551. Fax: +1(415) 502-2663. E-mail: Christopher.gordon@oarg.ucsf.edu

Introduction

It is well established from population studies that bone density can be a reliable indicator of the risk of vertebral fracture. However, from reviews of several case–control trials it is also known that bone mass shows considerable overlap between groups of subjects who are well matched apart from the presence or absence of a vertebral fracture [1–3]. This overlap means there are other factors which contribute to the risk of vertebral fracture for a given subject. One of the most likely of these factors is the architecture of trabecular bone [4–6]. This means that it is not only the amount of mineral present that is important in resisting the forces transmitted to the bone but also the way that the mineral is arranged. Therefore to understand the mechanism by which variations in trabecular architecture can affect vertebral strength, architecture must be quantified at the spine.

Quantitative computed tomography (QCT) can be performed on clinical CT scanners to determine the true volumetric density of trabecular bone at the spine. It requires that an external bone mineral reference phantom be scanned along with the patient to calibrate the

Hounsfield numbers into bone mineral equivalent values. QCT can provide much valuable information to assess vertebral fracture risk [7–11] and with little or no increase in time and cost, a high-resolution CT scan can be included when QCT is performed to measure density. If this high-resolution scan is appropriately processed it may provide significant information about the structure of trabecular bone that may be a useful adjunct to the BMD measurement. However, to be judged useful, assessments of trabecular structure in vivo should enhance differences between fractured and non-fractured populations with low bone mass to allow better prediction of fracture risk.

The goal of this study was to assess whether an assessment of vertebral trabecular structure from a high-resolution CT image could be a useful adjunct to bone mineral density (BMD) measured using spinal QCT. First, we describe the protocol used to acquire the high-resolution CT images and then describe an algorithm to segment the trabecular bone from the soft tissue background. We then outline various indices that can be derived from the processed image and assess the relationship between these structure parameters and QCT-determined BMD. We end by examining the degree to which the trabecular structure measures differentiate two groups of subjects diagnosed with osteoporosis and matched apart from the presence or absence of a vertebral fracture.

Materials and Methods

Study Subjects

A total of 61 women enrolled in an ongoing clinical trial were examined. Each woman had a low BMD (T_{hip} or T_{spine} <–2.5) as determined by dual-energy X-ray absorptiometry (DXA). Twenty women had sustained a vertebral fracture as determined from conventional radiographs. Each subject was assessed for trabecular density and structure within 3 months of being screened by DXA, undergoing radiography to determine fracture status, and before commencing treatment. Table 1 gives the age, height and weight distributions of the fractured and non-fractured subjects.

Table 1. Comparison between the vertebral fracture group and the non-fractured controls, based on the mean ± 1 SD in age, height and weight .

	Fracture group (n=20)	Non-fracture controls (n=41)
Mean age (years)	71.6 ± 4.1	69.4 ± 5.1
Mean height (cm)	159.4 ± 8.5	159.8 ± 7.5
Mean weight (kg)	63.4 ± 9.1	63.0 ± 10.9

Image Acquisition

All study subjects were evaluated for trabecular density and structure on a GE CT-9800Q whole-body computed tomography system using the following CT scanning protocol. First, subjects had a volumetric QCT examination [12] using a low-dose technique (80 kVp, 140 mAs) that employed contiguous 3 mm slices to encompass L1–2. During the examination, an external BMD reference phantom was employed to relate the Hounsfield numbers in the CT image to grams of hydroxyapatite. After an assessment of density, a high-resolution CT technique was employed to image the trabecular structure at the midpoint of L1 and L2. With this technique (120k Vp, 340 mAs) the high-resolution image was acquired with a slice thickness of 1.5 mm and the field of view was reduced to yield an image matrix with a pixel size of 0.31 mm. The whole-body equivalent dose received by each subject from the volumetric QCT and high-resolution CT examination, combined, was approximately 160 μSv.

Image Segmentation

The objective in postprocessing the high-resolution QCT images was to segment the trabecular bone from the original cross-sectional image and represent its structure by a simplified image from which various indices expressing its mechanical competence can be extracted. The only intervention required by the user during this analysis was the placement of a line separating the spinal canal from the vertebral body. Once this line has been selected the algorithm proceeds automatically through the following steps. First, the boundary between cortical bone and the soft tissue background was defined using an automatic contour detection scheme [13]. A shrunken version of this outer contour was then used to represent an inner contour separating cortical bone from trabecular bone. Figure 1B shows the effectiveness of the contour algorithm. Once the inner contour was determined, trabecular bone was separated from the marrow background using an adaptive threshold adjusted to ignore intensity variations in marrow. This thresholding scheme generated a binary representation of the bone structure by comparing each pixel in the original gray level image to the corresponding pixel in a low-pass filtered version of itself [14]. Low-pass filtering was achieved by four applications of a 3×3 averaging mask. However, the adaptive threshold was sensitive enough to falsely identify small intensity variations in marrow as trabecular bone. Therefore a second threshold was applied to eliminate those pixels with a signal intensity consistent with the soft tissue background but identified as part of the trabecular bone network. This second threshold was defined as follows. First, an area of interest was defined in the spinal canal of each subject. The Hounsfield number corresponding to 2 standard deviations (SD) above the mean Hounsfield number in the soft tissue area defined within the spinal canal was

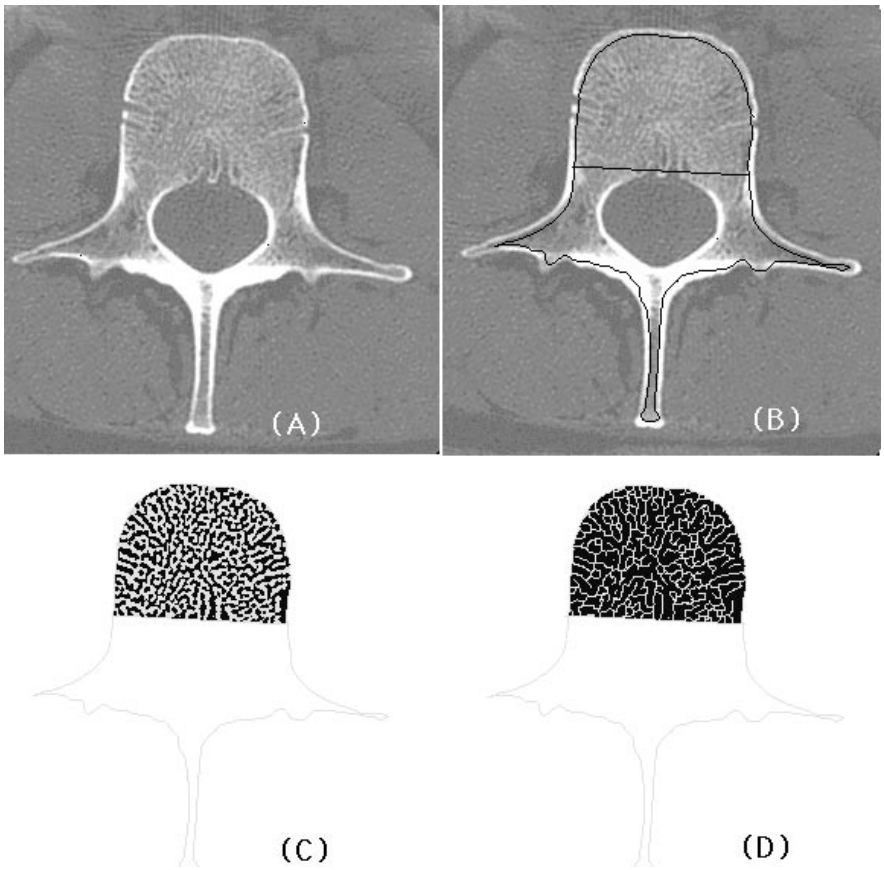

Fig. 1. The postprocessing steps used to assess trabecular structure from a high-resolution CT image (A) are shown. The structure is segmented by defining the boundry between cortical and trabecular bone (B). The trabecular network is reduced to a binary image (C) which is then thinned to produce a representation of the trabeculae from which connectivity can be assessed (D).

calculated and considered to be the second threshold for that subject. Setting this second threshold at 2 SD above the soft tissue background ensures that less than 2.5% of any soft tissue noise will be counted as bone.

After thresholding, a binary representation of the trabecular bone structure in the vertebral body was obtained. Figure 1C shows an example of this binary representation. As shown, the trabecular bone network in the original image is reasonably reproduced. A final representation of the structural shape of the vertebral trabecular structure was obtained by applying a skeletonizing algorithm [15] to the binary image. From this skeleton representation various indices of trabecular connectivity can be extracted. The results of applying the algorithm are shown in Fig. 1D.

Indices of Structure

We derived indices of structure to characterize vertebral size, apparent trabecular bone fraction, trabecular thickness, trabecular spacing and network connectivity. For each subject and for each structural parameter the average of L1 and L2 was calculated to indicate structural integrity. Vertebral size was quantified by the cross-sectional bone area (CSA) and was defined as the area within the inner contour selected by the postprocessing algorithm (Fig. 1B). Trabecular bone fraction (BV/TV), trabecular thickness (I.Th) and trabecular spacing (I.Sp) were derived from the binary image (Fig. 1C) using the run-length encoding steps suggested and applied to high-resolution CT images by Durand and Ruegsegger [16]. The run-lengths were encoded at 0° (across the image) and 90° (down the image). The average of these two directions was then used to calculate the structural parameters.

Using the star volume index, histological studies have shown that the number and size of holes in the trabecular bone network can reveal information about the netrwork's structural competence [17]. Basically, the star volume measure of the marrow space can be thought of as an application of run-length encoding in all possible directions. In previous work [18,19], we extended this approach in vivo by using a region-growing algorithm to extract the number and area of holes present in binary representations of the trabecular bone network. To locate the holes, the background in the binary image was considered to be a connected region that could be marked using region growing [14]. The number of regions grown defines the number of holes in the binary image. An account of the area of each hole is kept so that a mean (H_A) and maximum (H_M) hole size can be determined. To illustrate this consideration of the marrow space a hypothetical trabecular network is sketched in Fig. 2A. Eleven holes are present in this network. The hole with the largest area is also indicated.

Trabecular strut analysis was applied to quantify the degree of connectivity of the bone architecture

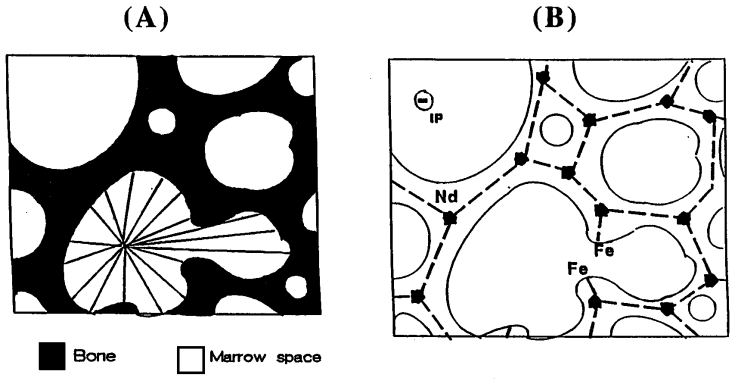

Fig. 2 a. A measurement of hole area by region growing is indicated. From a seed point, a hole is grown outward and isotropically until intersecting a trabecular bone boundry. **b.** Trabecular strut analysis of the two-dimensional trabecular bone structure. The bone network is represented by a series of one-dimensional struts shown here as broken lines. Junctions in the network are indicated by nodes (Nd) and discontunities by free ends (Fe) and isolated points (Ip).

represented in the skeleton image (Fig. 1D). In trabecular strut analysis, the discriminating parameters for structure are the number of nodes (Nnd), free ends (Nfe), isolated points (Ip) and network length (Nl). These parameters are shown in Fig. 2B and represent, respectively, the junction of three or more trabeculae, those trabeculae that are only attached to a junction at one end, trabeculae running perpendicular to the image plane, and the total length of the skeleton network. From these trabecular strut parameters, a well-connected bone is characterized by a large number of nodes and few free ends. This arises because disruptions in the bone network such as breaks along a strut increases the free end number by 2 for every break that occurs.

Statistical Analysis

Differences between the vertebral fracture group and the non-fractured controls were described using percent decrements. Significant differences between the group means were tested using Student's *t*-test, with statistical significance set at $p = 0.05$. Pearson correlations were used to assess the relationship between the structural parameters and BMD. Odds ratios were calculated to estimate the odds of a vertebral fracture occurring for every 1 SD change in BMD or each structural parameter. The 95% confidence interval was also calculated for each odds ratio. The significance of the independent contribution of each structural parameter to fracture risk was explored by logistic regression. This was done entering BMD followed by a structural parameter into a linear regression model to predict fracture outcome.

The ability of QCT-determined BMD and structural parameters to discriminate between the control subjects and women with vertebral fracture was evaluated by using the receiver operating characteristic (ROC) approach. The ROC curve plots the true positive fraction (TPF) (sensitivity) against the false positive fraction (FPF) (one minus specificity) by successively changing the cutoff threshold used to separate the two study populations. For all variables except I.Sp and H_A, sensitivity was defined as the total number of subjects with a fracture below the threshold divided by the total number of subjects with a fracture. Similarly, specificity was defined as the total number of non-fractured control subjects with a value above the threshold divided by the total number of non-fractured controls. In the case of I.Sp and H_A, sensitivity was defined by the total number of fracture subjects above the threshold because with disruptions in the trabecular network, larger holes are created. Specificity based on I.Sp and H_A was defined as the proportion of control subjects below the cutoff point. For ROC analysis the measurement with the greatest area under the curve has the highest discriminating ability between fractured and non-fractured subjects. That is, a test that completely separates normal from abnormal subjects would have an ROC curve in the upper left corner of the plot, indicating an area under the curve of 100%. The area and significant differences in area under the curves for BMD and structural parameters were calculated using the CALIBROC program of Metz [20].

Results

Reproducibility

For all practical purposes, the values of the indices of structure were not dependent on the variability with which an operator placed the line segment separating the vertebral body from the spinal canal. For example, as examined by the placement of this line segment five times in a given image, all indices of trabecular structure changed less than 1%.

A second issue of reproducibility concerned the variability of the threshold used to segment trabecular bone from the soft tissue background. To check this variability the mean threshold value of the 41 control subjects was calculated. The mean soft tissue threshold derived in each of the 20 fracture cases was also calculated and was not different (< 0.2%) from the mean value calculated from the control group. The coefficient of variation associated with each of these mean threshold values was also small (< 2%).

Table 2. Correlation between QCT BMD and indices of structure (R_{BMD}) and between indices of structure derived from L1 and L2 ($R_{L1,L2}$)

Structural index	R_{BMD}	$R_{L1,\ L2}$
BV/TV	0.79	0.84
I.Th	0.65	0.78
I.Sp	–0.78	0.84
H_A	–0.70	0.77
H_M	–0.78	0.87
Nl	0.56	0.82
Nnd	0.73	0.80
Nfe	–0.64	0.84
Nip	–0.64	0.77

For explanation of structural indices see the text.
All correlations are significant at $p < 0.0001$

Correlations

Pearson correlations between the parameters of trabecular bone structure and QCT BMD are listed in Table 2. The correlations between the structural parameters derived from L1 and L2 are also listed in Table 2. All structural parameters were correlated with BMD with $p < 0.0001$. BV/TV, I.Sp and H_M had the highest correlations with BMD. The structural parameters derived from the skeletonized representation of the trabecular bone network had the lowest correlation with BMD. However, the correlation coefficients for BV/TV, I.Sp and H_M with BMD were not statistically different ($p > 0.3$) from the correlation coefficients between BMD and those parameters extracted from the skeletonized network. The structural parameters estimated from L1 were strongly associated with those derived from L2 ($R_{L1,L2} > 0.76$, $p < 0.0001$). This agreement between L1 and L2 confirms that an average of L1 and L2 is a good indicator of overall vertebral trabecular structure.

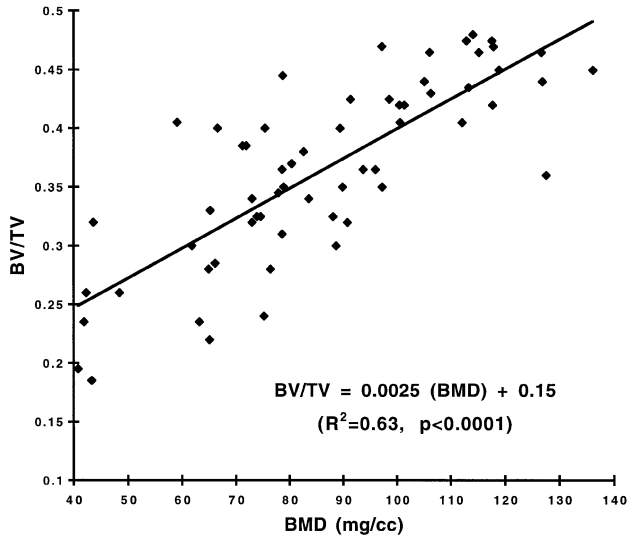

Fig. 3. Relationship between QCT determined BMD and the trabecular bone fraction (BV/TV). The regression line corresponds to least squares fit to all 61 points.

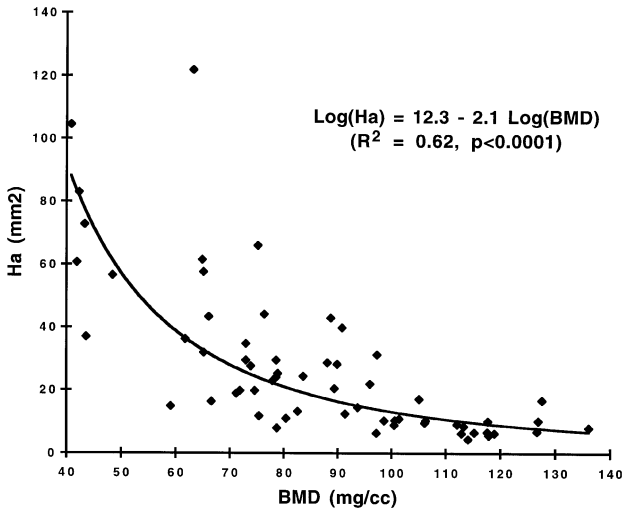

Fig. 4. Relationship between QCT determined BMD and the mean hole size (H_A).

Plots of BV/TV and H_A versus BMD for all 61 subjects are shown in Fig. 3 and Fig. 4, respectively. As shown, the bone fraction varies directly with BMD while hole size decreased non-linearly with increasing BMD. When transformed to a log-log scale, a least squares fit to the data revealed that H_A was strongly related ($r = 0.79$, $p < 0.0001$) to the reciprocal of BMD raised to the power of 2.1. This reciprocal fit is also plotted with the data.

Indices of trabecular structure were intercorrelated. For example I.Th and I.Sp showed a strong correlation with BV/TV ($0.92 < r < 0.96$, $p < 0.0001$) while H_A and H_M were also strongly correlated with BV/TV ($–0.90 < r < –0.88$, $p < 0.0001$). Measures of the inter-trabecular space also correlated well. For example, I.Sp showed a strong correlation with H_A ($r = 0.92$, $p < 0.0001$) and H_M ($r = 0.84$, $p < 0.0001$).

Vertebral Fracture Discrimination

Inter-group differences and levels of significance between the vertebral fracture subjects and the non-fractured controls are summarized in Table 3. Five points are worth noting from this table. First, although the study subjects were preselected to have a low BMD based on a DXA spine or hip measurement, QCT-determined BMD was strongly associated with fracture status. Second, in general the variance associated with the mean of the structural parameters increased in the fractured group in comparison with the non-fractured controls. Third, the largest percent and significant difference between the two groups was indicated by the hole size measure H_A. Fourth, the odds ratios indicate that, along with BMD, a 1 SD change in each of the structural parameters results approximately in a 2-fold increase in vertebral fracture risk. Fifth, all structural parameters showed significant ($p < 0.03$) differences between the two groups. Most importantly, however, except for H_A, none of the differences in

Table 3. Mean differences (% △), *t* value, odds ratios (95% confidence intervals) and levels of significance (*p*) between the vertebral fracture subjects (Fx) and the non-fractured controls (Non-Fx)

	Non-Fx Mean ± 1 SD	Fx Mean ± 1 SD	% △	*t*	Odds ratio (95% CI)	*p*
BMD (mg/cm^3)	92.95±20.9	73.17±24.8	–21.3	3.3	2.33 (1.30, 4.19)	0.005
CSA (mm^2)	705.29±122.3	746.54±156.1	5.8	–1.1	1.33 (0.81, 2.19)	0.26
BV/TV	0.39±0.06	0.32±0.09	–18.0	3.6	2.21 (1.33, 3.68)	0.002
I.Th (mm)	0.59±0.04	0.55±0.06	–5.9	3.2	1.63 (1.03, 2.57)	0.005
I.Sp (mm)	0.93±0.17	1.19±0.37	28.6	–3.8	1.91 (1.26, 2.89)	0.002
H_A (mm^2)	18.64±11.5	44.90±33.6	141.9	–4.5	1.94 (1.29, 2.90)	0.001
H_M (mm^2)	325.97±177.3	470.85±196.3	44.7	–2.9	2.13 (1.21, 3.76)	0.009
Nl	374.47±69.7	304.59±86.8	–18.7	3.4	2.56 (1.36, 4.83)	0.004
Nnd	79.29±32.2	47.54±33.9	–40.2	3.5	3.03 (1.47, 6.26)	0.003
Nfe	125.13±44.8	157.27±57.1	25.7	–2.4	1.77 (1.07, 2.93)	0.03
Nip	19.58±14.8	32.55±20.1	60.0	–2.8	1.89 (1.16, 3.09)	0.01

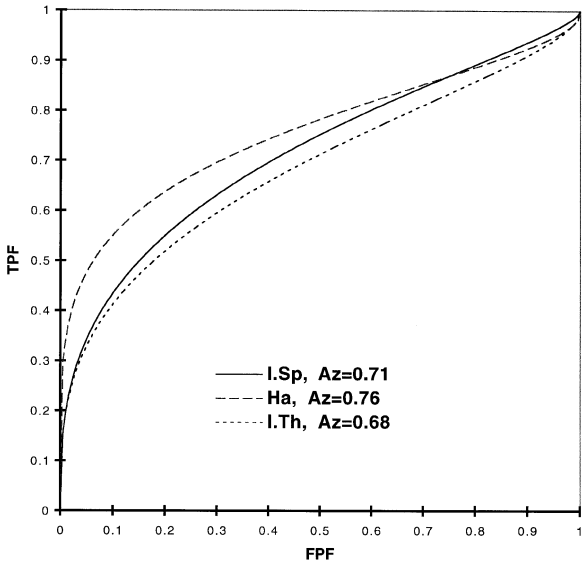

Fig. 5. The ROC curves for H_A, I.Sp and I.Th. The area under each curve (Az) is significantly different from that under a diagonal line (area = 0.5) indicating that each parameter could differentiate vertebral fractured subjects from non-fractured controls.

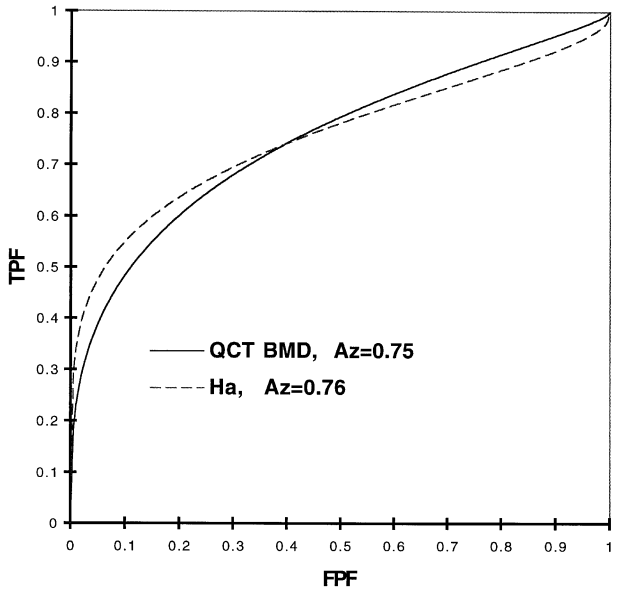

Fig. 6. The ROC curves for BMD and H_A. The curves cross at a FPF > 0.5 because 9 of the 41 non-fractured controls had a BMD value between 112 mg cm^{-3} and 119 mg cm^{-3}. The area under each curve is given by Az.

trabecular structure parameters remained significant after adjustment of the data for BMD. When BMD and then H_A were entered into a paired linear regression model to predict fracture outcome, H_A contributed with a *p* value of 0.03 while BMD had an associated *p* value of 0.86.

The size of the intertrabecular space was characterized by H_A and I.Sp. To compare the diagnostic value of these two means of assessing the intertrabecular space, the ROC curve for each is shown in Fig. 5. The ROC curve for I.Th is also shown for comparison. The area under each curve, an index of the ability of a test to detect vertebral fractures, is 0.76 ± 0.07 for H_A, 0.71 ± 0.07 for I.Sp, and 0.68 ± 0.08 for I.Th. For all three curves the areas are significantly different ($p < 0.05$) from a diagonal line, indicating that each is an effective test. The H_A ROC curve was significantly different from that for I.Sp ($p = 0.05$) but just failed to be significantly different from I.Th ($p = 0.07$).

The ROC curves for H_A and BMD are shown in Fig. 6. The areas under the curves are 0.75 ± 0.07 for BMD and 0.76 ± 0.07 for H_A. Although the areas under the two curves are not different ($p = 0.47$), H_A separated the two groups with greater sensitivity for high degrees of specificity (false positive fraction <0.2). The benefit of this increased sensitivity is illustrated in Figs 7 and 8. Figure 7 shows a significant overlap between the trabecular bone density in the non-fractured and fractured group. Figure 8 shows that this overlap between the two groups is reduced by H_A, resulting in improved differentiation of fracture subjects from the control subjects.

Figure 9 shows the thinned binary representation of the trabecular bone structure at the midpoint of the L1 vertebrae of a 70-year-old woman without a vertebral fracture and a 69-year-old woman who suffered a vertebral fracture. For a 6% difference in QCT-determined trabecular BMD there is a 5-fold difference in H_A. Differences were also apparent for other structural

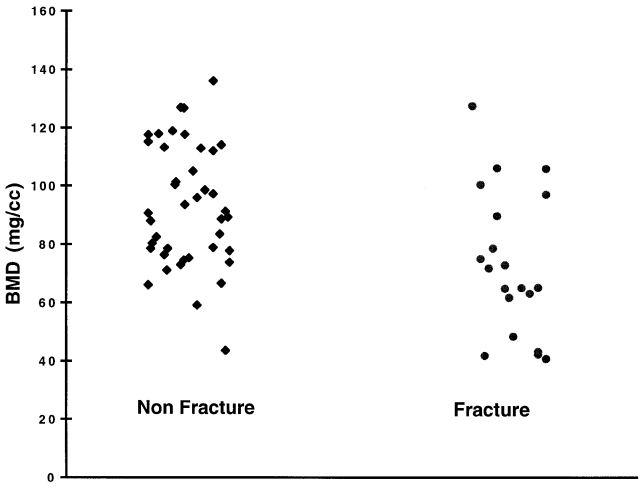

Fig. 7. Comparison of the range of trabecular bone densities recorded in the non-fractured controls and the vertebral fracture subjects. The mean density of the fracture group is 21% lower than the mean density of the control group.

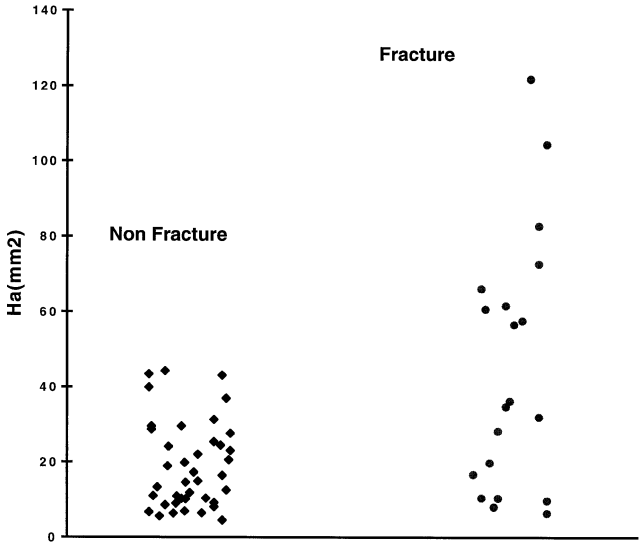

Fig. 8. The discrimination of the non-fractured controls and the vertebral fracture subjects based on a measurement of H_A. The mean H_A of the fracture group is 142% greater than that of the non-fractured controls.

indices. For example, BV/TV and I.Th for the non-fractured subject is 0.37 and 0.57 mm, respectively. The values decrease to 0.24 and 0.47 mm in the vertebral fracture subject.

Discussion

Although the risk of fracture increases as bone mass decreases, variations in trabecular structure can also affect bone strength and should also be quantified in vivo. To obtain information concerning the structure of trabecular bone in vivo, two requirements must be met: to image the structure of bone at a clinically relevant site and to quantify the imaged structure. QCT was developed to determine trabecular BMD predominantly at the spine and can satisfy both these requirements [21]. A determination of BMD by QCT at the spine requires the performance of calculations on the image matrix. If the CT image matrix is reconstructed over a small field of view the trabecular pattern is revealed. In principle, the spatial resolution required to quantitate the structure of trabecular bone is dictated by the dimensions of the trabecular lattice. Histomorphometric studies have shown that this lattice consists of a network of rods and plates. The rods have a diameter of about 0.2 mm and interconnect with the plates to produce trabecular spaces of cross-sectional area of about 0.75 mm $\times$ 1 mm [22,23]. In practice, the spatial resolution achievable in vivo on current whole-body imagers is just sufficient to reveal some of the structural pattern in the vertebral body. This pattern is limited by the fact that projections blur the bone structure in the final image. This blurring arises because the minimum slice thickness achievable (~ 1 mm) in vivo is 3–5 times thicker than the average trabecular width and about equal to the average intertrabecular dimension found in normal subjects. However, with the aid of image processing methods various indices quantifying the structure and texture of the imaged bone can be derived. The mechanical integrity of the trabecular network is then inferred from these indices.

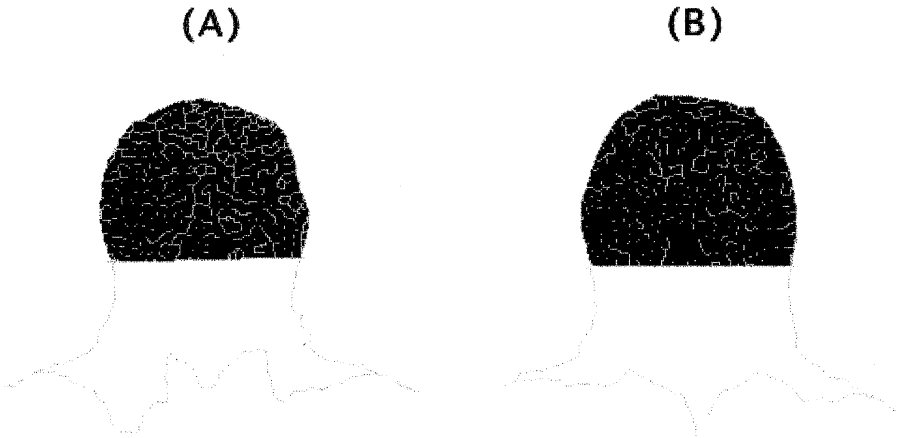

Fig. 9. This figure shows the thinned binary representation of the connectivity in the trabecular network of a 70 year old woman with a QCT BMD of 80.4 mg cm^{-3} and without a vertebral fracture (A) and a 69 year old woman with a BMD value of 75.2 mg cm^{-3} who experienced a vertebral fracture (B). An H_A value of 13.8 mm^2 was determined for the non-fractured subject and 66.1 mm^2 for the fractured subject.

In this study we acquired a high-resolution CT image at the midpoint of L1 and L2 in a group of subjects having spinal QCT. The high-resolution images were then postprocessed to segment trabecular bone from the soft tissue background, and indices to quantify trabecular thickness, intertrabecular spacing and the network connectivity were measured. The measured structural parameters were all strongly correlated with QCT-determined BMD. All parameters could be determined with an intra-observer variability consistent with precision errors reported for a determination of trabecular bone density of the lumbar vertebrae by QCT (2–4%) [24,25]. The structural parameters also reflected known patterns of bone loss established from biopsy studies. For example, in the normal aging process bone mass is lost from trabecular bone due to entire trabeculae being removed rather than by a generalized uniform thinning of the whole trabecular structure [5,26]. The remaining trabeculae are more widely separated, less connected, and therefore less likely to resist a compressive force. Comparable differences were noted in the women we studied. First, there was a slight but significant decrease (7%) in the mean trabecular thickness in the vertebral fracture group in comparison with the non-fractured controls. However, with the limits imposed by the image resolution and slice thickness, this trabecular thickness parameter must be viewed as reflecting the apparent trabecular size only as it appears in the CT image. Second, the variances associated with the means of the structural parameters were, in general, larger in the fractured group. We interpret this increased variance as an indication of a more disrupted network that eventually leads to fracture. Third, there was a significant increase in the size of the intertrabecular space in subjects with vertebral fractures. This increase in the intertrabecular space was better indicated by H_A than I.Sp.

To obtain the mean hole size, H_A, the number and area of each hole present in the binary representation of the trabecular structure is recorded. Although the majority of holes are only a few pixels in area the presence of a few large holes resulting from breaks in the bone network skews the average value. Therefore, H_A will be very sensitive to small changes in the trabecular bone network not readily detected by a measurement of bone mass. This is important because the mechanical integrity of a trabecular bone structure can vary by an order of magnitude with apparently small redistributions of mineral without a substantial change of mass [23]. When applied to high-resolution peripheral quantitative computed tomography (pQCT) images of the distal radius, the H_A index differentiated a small group of Colles' fracture subjects from the normal population better than a pQCT-determined trabecular or cortical density [18]. Also, when applied to high-resolution magnetic resonance images of the distal radius the index of hole size reflected known age-related changes in trabecular bone structure [19].

Previous work using thin-slice high-resolution CT to quantify trabecular bone structure in vivo assessed connectivity from a skeletonized representation of the trabecular network [27]. These authors suggested a feature termed the trabecular fragmentation index, which reflected the number of free ends and isolated points in the bone network. This fragmentation index was able to separate osteoporotic subjects from normal subjects but performed poorly when applied to separating postmenopausal osteoporotic women with vertebral fractures from those without fracture. An assessment of vertebral structure based on parameters derived from run-length encoding has also been reported [28,29]. In these works a textural index quantifying the intertrabecular space was helpful in the assessment of fracture risk, but only in elderly women who had very low (< 50 mg cm^{-3}) QCT-determined BMD values. As it assesses the intertrabecular space from run-length encoding, this texture index derived by Ito et al. is comparable to our index of hole size, I.Th. However, in this work we have used ROC analysis to show that the diagnostic value of an assessment of the intertrabecular space by I.Th can be improved by extending the run-length encoding steps to all possible directions. This was done and supplied our index H_A. Interestingly, from the non-linear relationship between BMD and H_A we have noted in Fig. 4, it is not surprising that an index to quantify the intertrabecular space will be helpful in assessing fracture risk, especially in subjects with very low BMD values. As shown in Fig. 4, small decrements in BMD are magnified by H_A. The comparison of the two subjects shown in Fig. 9 indicates that this magnification may be clinically important in certain cases. Once identified, subjects with such structural deficiencies may be targeted with more aggressive therapies.

In this study it was not surprising that QCT-determined BMD was one factor that was highly associated with fracture status. However, a significant finding was the enhanced mean difference between the vertebral fracture subjects and the non-fractured controls due to an assessment of trabecular bone structure from a high-resolution CT image. This was true of almost all structural parameters derived. For example, in the two populations examined, a measure of BMD revealed that the fracture group had a 21% lower BMD than the non-fractured controls. Greater differences were recorded for H_A (142%), H_M(44%) and Nnd (40%). However, logistic regression revealed that only H_A appeared to contribute significant information independent of BMD. ROC analysis revealed that the information contributed by H_A resulted from the fact that for a high degree of specificity (false positive fraction < 0.2) the groups could be discriminated with a greater degree of sensitivity than achievable with BMD. This increased sensitivity was clearly indicated in Fig. 8.

The fact that an assessment of structure can enhance differences between two groups of subjects diagnosed with osteoporosis and well matched apart from the presence or absence of a vertebral fracture is clinically valuable from two standpoints. First, in populations identified with low bone mass future fractures are at least partially preventable by interventions such as estrogen

[30,31] and bisphosphonate therapies [32,33]. Second, knowledge of the presence of a reduced bone mass has been shown to influence behavior in ways that reduce the impact of detrimental lifestyle factors associated with an increased fracture risk [34]. The same positive effects are likely to occur with the discriminating information provided by image-based assessments of trabecular bone structure.

In conclusion, our results suggest that an assessment of vertebral trabecular structure from high-resolution CT images is a useful adjunct to QCT-determined BMD because the structural parameters can potentially enhance differences between subjects with or without a vertebral fracture and with overall low density. We are currently evaluating our study population after 2 years of treatment. This will provide further insight into the clinical usefulness of longitudinal image-based assessments of trabecular bone structure.

Acknowledgements. This research was partially supported by Pfizer and Eli Lilly and Company.

References

1. Mazess RB. On aging and bone loss. Clin Orthop 1981;165:239–52.
2. Cummings SR. Are patients with hip fractures more osteoporotic? Review of the evidence. Am J Med 1985;78:487–94.
3. Ott SM. When bone mass fails to predict bone failure. Calcif Tissue Int 1993;53(Suppl 1):S7–13.
4. Townsend PR, Raux P, Rose RM, Miegel RE, and Radin EL. The distribution and anisotropy of the stiffness of cancellous bone in the human patella. J Biomech 1975;8:363–7.
5. Kleerekoper M, Villanueva AR, Stanciu J, Sudhaker D, Parfitt AM. The role of three-dimensional trabecular microstructure in the pathogenesis of vertebral compression fractures. Calcif Tissue Int 1985;37:594–7.
6. Goldstein SA. The mechanical properties of trabecular bone: dependence on anatomic location and function. J Biomech 1987;20:1055–61.
7. Cann CE, Genant HK, Kolb FO, Ettinger B. Quantitative computed tomography for prediction of vertebral fracture risk. Bone 1985;6:1–7.
8. Heuck AF, Block J, Gluer CC, Steiger P, Genant HK. Mild versus definite osteoporosis: comparison of bone densitometry techniques using different statistical models. J Bone Miner Res 1989;4(6):891–900.
9. Guglielmi G, Grimston SK, Fischer KC, Pacifici R. Osteoporosis: diagnosis with lateral and posteroanterior dual x-ray absorptiometry compared with quantitative CT. Radiology 1994;192:845–50.
10. Laval-Jeantet AM, Bergot C, Williams M, Davidson K, Laval-Jeantet M. Dual-energy absorptiometry of the calcaneus: comparison with vertebral dual-energy x-ray absorptiometry and quantitative computed tomography. Calcif Tissue Int 1995; 56:14–8.
11. Grampp S, Genant HK, Mathur A, Lang P, Jergas M, Takada M, et al. Comparison of noninvasive bone mineral measurements in assessing age-related loss, fracture discrimination, and diagnostic classification. J Bone Miner Res 1997;12:697–711.
12. Lang TF, Keyak JH, Heitz MW, Augat P, Lu Y, Mathur A, Genant HK. Volumetric quantitative computed tomography of the proximal femur: precision and relation to bone strength. Bone 1997;21:101–8.
13. Robinson GS. Edge detection by compass gradient masks. Comput Graphics Image Process 1977;6:492–501.
14. Gonzalez WC, Woods RE. Digital image processing. Reading: Addison-Wesley, 1992:chaps 4,7.
15. Zhany TY, Suen CY. A fast parallel algorithm for thinning digital patterns. Commun Assoc Comput Mach 1984;27:236–9.
16. Durand EP, Ruegsegger P. Cancellous bone structure: analysis of high-resolution CT images with the run-length method. J Comput Assist Tomogr 1991;15:133–9.
17. Vesterby A, Mosekilde L, Gundersen HJG, Melsen F, Mosekilde L, Holme K, Sorensen S. Biologically meaningful determinants of the in vitro strength of lumbar vertebrae. Bone 1991;12:219–24.
18. Gordon CL, Webber CE, Adachi JD, Christoforou N. In-vivo assessment of trabecular bone structure at the distal radius from high-resolution computed tomography images. Phys Med Biol 1996;41:495–508.
19. Gordon CL, Webber CE, Christoforou N, Nahmias C. In vivo assessment of trabecular bone structure at the distal radius from high-resolution magnetic resonance images. Med Phys 1997; 24:585–93.
20. Metz CE. CALIBROC: program to calculate the statistical significance of the difference between two estimated ROC curves. Department of Radiology, University of Chicago, 1988.
21. Cann CE, Genant HK. Precise measurements of vertebral mineral content using computed tomography. J Comput Assist Tomogr 1980;4:493–500.
22. Amstutz HC, Sissons HA. The structure of vertebral spongiosa. J Bone Joint Surg Br 1969;51:540–50.
23. Jensen KS, Mosekilde L, Mosekilde L. A model of vertebral trabecular bone architecture and its mechanical properties. Bone 1990;11:417–23.
24. Laval-Jeantet AM, Genant HK, Wu CY, Gluer CC, Faulkner KG, Steiger P. Factors influencing long-term in vivo reproducibility of QCT vertebral densitometry. J Comput Assist Tomogr 1993;17:915–21.
25. Genant HK, Engelke K, Fuerst T, Gluer C, Grampp S, Harris S, et al. Noninvasive assessment of bone mineral and structure: state of the art. J Bone Miner Res 1996;11:707–30.
26. Parfitt AM, Mathews CH, Villanueva AR, Kleerekoper M. Relationship between surface, volume, and thickness of iliac trabecular bone in aging and in osteoporosis. J Clin Invest 1983;72:1396–409.
27. Chevalier F, Laval-Jeantet AM, Bergot C. CT image analysis of the vertebral trabecular network in-vivo. Calcif Tissue Int 1992;51:8–13.
28. Ito M, Ohki M, Hayashi K, Uetani M, Yamada M, Nakamura T. Trabecular texture analysis of CT images in relationship with spinal fracture. Radiology 1995;194:55–9.
29. Ito M, Ohki M, Hayashi K, Yamada M, Uetani M, Nakamura T. Relationship of spinal fracture to bone density, texture, and anthropometric parameters. Calcif Tissue Int 1997;60:240–3.
30. Weiss NS, Ure CL, Ballard JH, William AR, Daling JR. Decreased risk of fractures of the hip and lower forearm with postmenopausal use of estrogen. N Eng J Med 1980;303:1195–8.
31. Kiel DP, Felson DT, Anderson JJ, Wilson PWF, Moskowitz MA. Hip fracture and the use of estrogens in postmenopausal women. N Eng J Med 1987;317:1169–74.
32. Storm T, Thamsborg G, Steiniche T, Genant HK, Sorenson OH. Effect of intermittent cyclical etidronate therapy on bone mass and fracture rate in women with postmenopausal osteoporosis. N Eng J Med 1990;322:1265–71.
33. Watts NB, Harris ST, Genant HK, Wasnich RD, Miller PD, Jackson RD, et al. Intermittent cyclical etidronate treatment of postmenopausal osteoporosis. N Eng J Med 1990;323:73–9.
34. Rubin SM, Cummings SR. Results of bone densitometry affect women's decisions about taking measures to prevent fractures. Ann Intern Med 992;116:990–5.

Received for publication 10 October 1997
Accepted in revised form 4 December 1997